

COMBINED EFFECTS OF MAGNETIC FIELD AND THERMAL RADIATION ON FLUID FLOW AND HEAT TRANSFER IN MOLTEN SALT

Panxin Li^{1,2*}, Jiajun Song², Lu Chen², Benwen Li², Christian Karcher¹

¹ *Institute of Thermodynamics and Fluid Mechanics, Technische Universitt Ilmenau, Ilmenau, Germany*

² *School of Energy and Power Engineering, Dalian University of Technology, Dalian, China*

*e-Mail: panxin.li@tu-ilmenau.de

The combined effects of magnetic field and thermal radiation on the fluid flow and heat transfer characteristics of two-dimensional Rayleigh–Bénard convection in molten salt are investigated numerically by using a collocation spectral method. A series of simulations are carried out for Rayleigh numbers between 10^5 and 10^6 , Hartmann number ranging from 30 to 100, and with the radiation-conduction parameter fixed between 0.5 and 4, respectively. For the computation of radiation field, we start from a simple model, named the linear Rosseland approximation [1], which assumes that the radiative heat flux is mainly diffusive and proportional to the temperature gradient. The results show that the convective heat transfer along the bottom wall is weakened under the combined influences of both magnetic field and thermal radiation. However, depending on the actual values of the parameters, the overall convective heat transfer and fluid flow can be either enhanced or suppressed under the combined effects.

Introduction.

With the gradual exhaustion of fossil energy and the deterioration of the ecological environment, the development and utilization of renewable and clean energy (such as solar energy, wind energy, biomass, and geothermal energy, etc.) have received a great deal of attention in the past decades. Among those resources, solar energy is regarded as the most promising source because it is widely distributed, abundant and pollution-free. However, due to the instability and intermittency of the process, the storage and conversion of solar energy becomes important. Molten salts [2, 3] are considered as the most common thermal energy storage materials which have favorable properties, such as the high boiling point, low viscosity, low vapor pressure and high specific heat capacity, etc. Since molten salts are electrically conducting and radiatively participating, considering the combined effects of the magnetic field and thermal radiation on fluid flow and heat transfer is crucial. A large number of studies focus on the fluid flow of molten salt [4–9]. For instance, Smolentsev *et al.* [5] analysed the effect of a wall-normal magnetic field on turbulent flow in molten salt. Wang *et al.* [7] investigated the effects of radiative transfer on the temperature distribution in a three-dimensional tube based on the finite element method. Guo *et al.* [6] studied the motion under the effects of a uniform and a non-uniform magnetic field. These studies demonstrate that both magnetic field and thermal radiation have crucial effects on the flow motion in molten salt. However, most of those works focus on the effect of the magnetic field, but only few of them pay attention to radiation. Therefore, in this paper, we focus on exploring the combined influences on heat transfer and fluid flow in the classical Rayleigh–Bénard convection (RBC) model. The findings are accessible in terms of the corresponding temperature and flow fields as well as the dependence of Nusselt and Reynolds numbers on the control parameters.

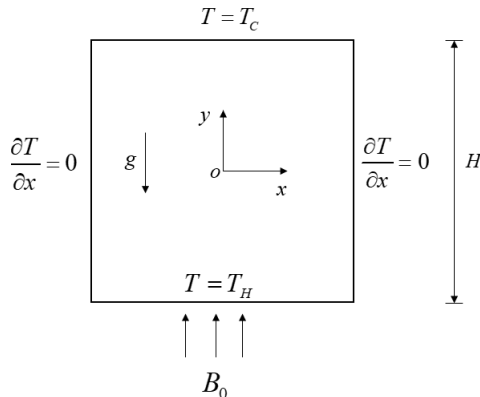


Fig. 1. Physical model.

Table 1. Physical properties of molten salt at $T_0 = 300^\circ\text{C}$ [10–12]

	Symbol	Value	Unit
Thermal diffusivity	α	1.888×10^{-7}	m^2/s
Thermal conductivity	λ	0.483	$\text{W}/(\text{mK})$
Density	ρ	1640	kg/m^3
Specific heat capacity	c_p	1560	$\text{J}/(\text{kg}\cdot\text{K})$
Kinematic viscosity	ν	1.927×10^{-6}	m^2/s
Absorption coefficient	β'	200	m^{-1}

1. Presentation of the problem.

Consider a square cavity as shown in Fig. 1, filled with electrically conducting molten salt. The physical properties of the molten salt at a temperature of 300°C are listed in Table 1. The lower wall is heated at a constant temperature T_H and the upper wall is cooled at a constant temperature T_C , where $\Delta T = T_H - T_C > 0$. The sidewalls are assumed as adiabatic. The distance between the upper and lower plates is H . Besides, all walls have no-slip velocity boundary conditions and are electrically insulated. An external vertical magnetic field at a constant and homogeneous flux density B_0 is applied. We apply the quasistatic approximation for a small magnetic Reynolds number, i.e. ignoring the effect of the induced magnetic field. Under these conditions, there is no electrical potential, i.e. we have $\phi = 0$. For the modeling of thermal radiation, we adopt the Rosseland approximation, which is suitable for an optically thick medium, $\tau \gg 1$, where $\tau = \beta' H$ and β' denotes the attenuation coefficient. Since the scattering is not considered, β' is identical to the absorption coefficient. Hence, the model assumes that the radiation power is completely attenuated within the cavity. The thermal radiation is coupled to convection via the radiative heat source term $-\nabla \cdot \mathbf{q}_R$ into the heat Rtransfer equation. To obtain it, several methods have been developed, e.g., P-N approximation, Rosseland approximation, and Discrete Ordinates Method (DOM). Compared with the other methods, solving the radiative transfer equation (RTE) using DOM provides more detail about the radiative heat transfer, but its solving is much more complicate and time-consuming. For the present work, we start from adopting a simple radiation model, i.e. the Rosseland approximation, which only suits for an optically thick medium. When

it is applied, the radiative heat flux \mathbf{q}_R is assumed to be proportional to the temperature gradient,

$$\mathbf{q}_R = -\frac{16\sigma T_0^3}{\beta' \nabla}, \quad (1)$$

where σ denotes the Stefan–Boltzmann constant, $\sigma = 5.67 \cdot 10^{-8} \text{ W}/(\text{m}^{-2}\text{K}^{-4})$, and T_0 represents the reference temperature, $T_0 = (T_H + T_C)/2$, while β' is the attenuation coefficient.

All physical parameters of the working fluid, e.g., the kinetic viscosity ν , the thermal diffusivity α , the thermal expansion coefficient β , the dynamic viscosity μ , the thermal conductivity λ , and the electrical conductivity σ are assumed to be constant except for the density changes with temperature under the buoyancy force. The Boussinesq approximation is employed.

Adopting H , α/H , $\rho\alpha^2/H^2$, H^2/α , B_0 , and T_0 as the reference scales for length, velocity, pressure, time, magnetic field strength and temperature, respectively, the dimensionless governing equations are derived as follows:

$$\frac{\partial U}{\partial X} + \partial V = 0, \quad (2)$$

$$\frac{\partial U}{\partial t} + U \frac{\partial U}{\partial X} + V \frac{\partial U}{\partial Y} = -\frac{\partial P}{\partial X} + \text{Pr} \left(\frac{\partial^2 U}{\partial^2 X} + \frac{\partial^2 U}{\partial^2 Y} \right) - \text{Pr Ha}^2 U, \quad (3)$$

$$\frac{\partial V}{\partial t} + U \frac{\partial V}{\partial X} + V \frac{\partial V}{\partial Y} = -\frac{\partial P}{\partial Y} + \text{Pr} \left(\frac{\partial^2 V}{\partial^2 X} + \frac{\partial^2 V}{\partial^2 Y} \right) + \text{Ra Pr } \Theta, \quad (4)$$

$$\frac{\partial \Theta}{\partial t} + U \frac{\partial \Theta}{\partial X} + V \frac{\partial \Theta}{\partial Y} = -(1 + N_R) \left(\frac{\partial \Theta}{\partial^2 X} + \frac{\partial \Theta}{\partial^2 Y} \right), \quad (5)$$

where $\Theta = (T - T_0)/(T_H - T_C)$ represents the dimensionless temperature. Besides, Pr , Ra , Ha and N_R and are the Prandtl number, the Rayleigh number, the Hartmann number and the radiation-conduction parameter, and their definitions are given as: $\text{Pr} = \nu/\alpha$, $\text{Ra} = g\beta\Delta TH^3/(\alpha\nu)$, $\text{Ha} = B_0 H \sqrt{\sigma/\mu}$, $N_R = 16\sigma T_0^3/(3\beta'\lambda)$. Here, it should be noted that when the radiative heat source term is obtained by solving RTE, the Planck number $\text{Pl} = \lambda/(4\sigma T_0^3 H)$ will be the key parameter to show the relationship between the radiative heat flux and the conductive heat flux. Pl is related to the radiation-conduction parameter $N_R = 4/(3\tau\text{Pl})$, where τ means the optical thickness, $\tau = \beta' H$, representing the transparency of the working fluid. The Prandtl number Pr denotes the ratio of two diffusive properties of the fluid, i.e. the kinematic viscosity as a measure of diffusion of momentum and the thermal diffusivity as a measure of diffusion of heat. Physically, Pr controls the relative thicknesses of the viscous and thermal boundary layers adjacent to rigid walls, where transport processes are dominated by diffusion. This implies that the thermal boundary layers are somewhat embedded in the viscous boundary layers. In the present study, Pr is fixed at the value 7. Note that the effect of the Prandtl number varying from 5 to 20 has already been investigated in previous work [8]. These results show that within this range, Pr has a minor influence on heat transfer and fluid dynamics. Besides, Ra is a measure of the flow-driving thermally induced buoyancy force, $10^5 \leq \text{Ra} \leq 10^6$. The corresponding temperature difference and the reference length for different the Ra numbers at a fixed reference temperature $T_0 = 300^\circ\text{C}$ are listed in Table 2. The Ha number represents the relative strength of the electromagnetically induced Lorenz

Table 2. Temperature difference and reference length for different Ra.

	ΔT	H
Ra = 10^5	0.01 K	0.06 m
Ra = 5×10^5	0.05 K	0.06 m
Ra = 10^6	0.10 K	0.06 m

Table 3. Grid independence tests at Ra = 10^6 , Ha = 0 and $N_R = 4$.

Grid	Nu_b^C	Re
40×40	4.6863 (-%)	61.8247 (-%)
50×50	4.6877 (0.03%)	61.8624 (0.06%)
60×60	4.6877 (0%)	61.8624 (0%)

force, and N_R represents the ratio of the radiative heat flux to the conductive heat flux. The dimensionless boundary conditions for temperature and velocity are as follows:

$$\begin{aligned} X = -0.5, X = 0.5, \partial\Theta/\partial X = 0, U = 0, V = 0, Y = 0.5, \\ \Theta = 0.5, U = 0, V = 0, Y = 0.5, \Theta = -0.5, U = 0, V = 0 \end{aligned} \quad (6)$$

Moreover, the definitions of the average convective Nusselt number along the bottom wall Nu_b^C , the average convective Nusselt number and the Reynolds number over the whole system, i.e. Nu^C and Re, are computed according to relations (7)–(9).

$$Nu_b^C = - \int_{-0.5}^{0.5} \frac{\partial\Theta}{\partial Y} \Big|_{Y=-0.5} dX, \quad (7)$$

$$Nu^C = 1 + \iint_{-0.5}^{0.5} V\Theta dXdY, \quad (8)$$

$$Re = \iint_{-0.5}^{0.5} \frac{1}{Pr} \sqrt{U^2 + V^2} dXdY \quad (9)$$

2. Results and discussion.

In order to solve the above equations, we adopt the collocation spectral method (CSM) to discretize the space and utilize the improved projection scheme (IPS) to decouple the velocity and pressure fields. Regarding the time discretization, the second-order forward difference scheme was adopted for the transient terms in Eqs. (3)–(5), the Adams–Bashforth scheme was used for the advection terms, and the implicit scheme was for the diffusion terms. As for the Lorentz force, buoyancy force and the radiative heat source terms, the explicit scheme was applied. A more detailed description of the detailed numerical method and solving steps are given in [7].

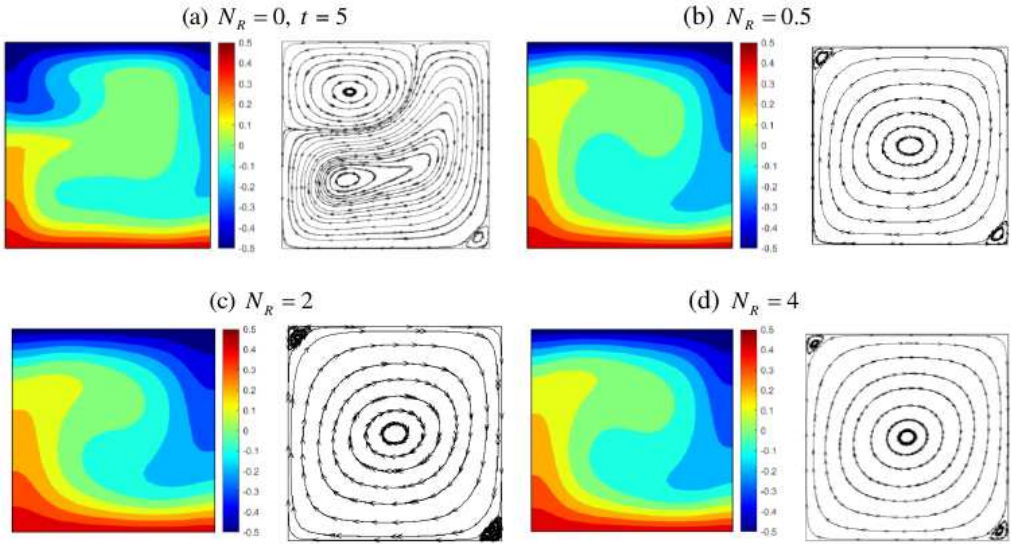


Fig. 2. Temperature distribution and streamlines for $Ra = 10^5$ and $Ha = 0$.

2.1. *Grid independence test and code validation.* The grid independence test has been conducted using three sets of meshes, consisting of 40×40 , 50×50 , and 60×60 collocation points, at $Ra = 10^6$, $Pr = 7$, $Ha = 0$ and $N_R = 4$. Finally, the balancing computation time and accuracy, the resolution of 50×50 were selected. A detailed validation procedure is likewise given in our previous work [8].

2.2. *Effects of thermal radiation.* In this section, we first explored the influence of thermal radiation on RB convection in the absence of a magnetic field, i.e. $Ha = 0$. Fig. 2 shows the temperature contours and streamlines for the cases of $Ra = 10^5$ when N_R varies from 0 to 4. The higher N_R shows that more thermal radiation is participated. Besides, it should be noted that for pure RB convection at $Ra = 10^5$ the fluid flow is time-dependent and in a periodic oscillatory state, which can be seen from our previous work [8]. In Fig. 2a, only the results at $t = 5$ is presented. However, when the thermal radiation is involved, we notice that the flow is stabilized to be a steady state at $N_R = 0.5$, $N_R = 0.2$ and $N_R = 4$. It indicates that the thermal radiation has a negative influence on the fluid motion. By comparing the results for $N_R = 0.5$, $N_R = 0.2$ and $N_R = 4$ in Fig. 2, it is clearly seen that the flow directions are the same and the flow patterns are similar. The hot fluid ascends from the left wall and the cold fluid descends from the right wall, so that one big vortex is formed in the cavity. In addition, there are two small vortices which are located in the top left corner and the bottom right corner.

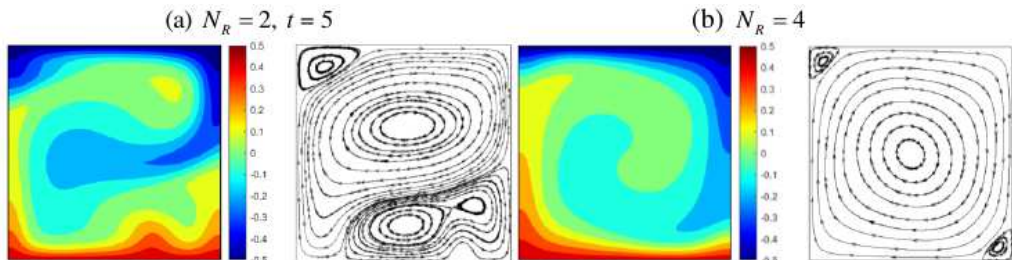


Fig. 3. Temperature distribution and streamlines for $Ra = 10^6$ and $Ha = 0$.

The temperature distributions and flow patterns at $Ra = 10^6$ when $N_R = 2$ and 4 are displayed in Fig. 3. Note that an irregular flow is observed at $N_R = 2$, and the results shown in Fig. 3a were obtained at a dimensionless time of 5. As N_R increases from 2 to 4, the convection becomes steady, which also suggests that the fluid flow is weakened by the involvement of thermal radiation.

2.3. Combined effects of magnetic field and radiation. Figs. 4–6 show the temperature contours and streamlines for the cases of $Ra = 10^5$, 5×10^5 and 10^6 at different N_R and Ha . As seen from Fig. 4a, for the case of $Ha = 30$ and $N_R = 2$, the flow pattern consists of two convective rolls with a downflow in the centre and an up-flow near the sidewalls. Both the temperature distribution and the streamlines are symmetrical with respect to the line $X = 0.5$. However, when Ha reaches 50, the temperature isotherms are parallel to the horizontal walls and there is no convective motion. This result implies that when compared to the buoyancy force the Lorentz force is predominant and the fluid flow is completely suppressed. And the heat transfer is mainly dominated by conduction.

When Ra increases to 5×10^5 , three long convective rolls are formed in the cavity that rotate in the counter- clockwise and clockwise direction, respectively. In this case, the temperature contours at $N_R = 2$ are no longer symmetrical as in Fig. 4a. However, there are two symmetrical large-scale rolls with two small secondary vortices located at the corners of the bottom plate at $Ha = 30$ and $N_R = 4$, as shown in Fig. 5c. With

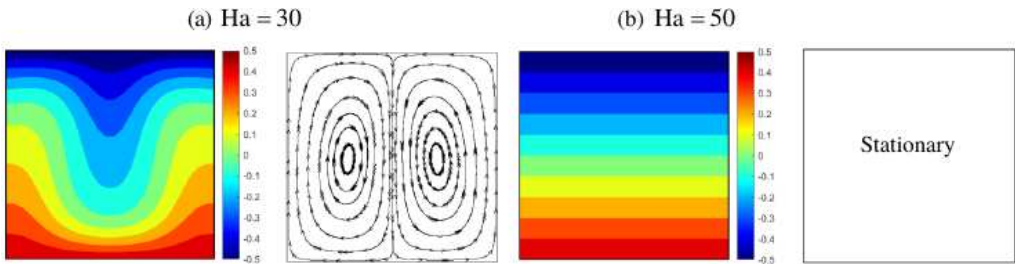


Fig. 4. Temperature distribution and streamlines for $Ra = 10^5$, $N_R = 2$.

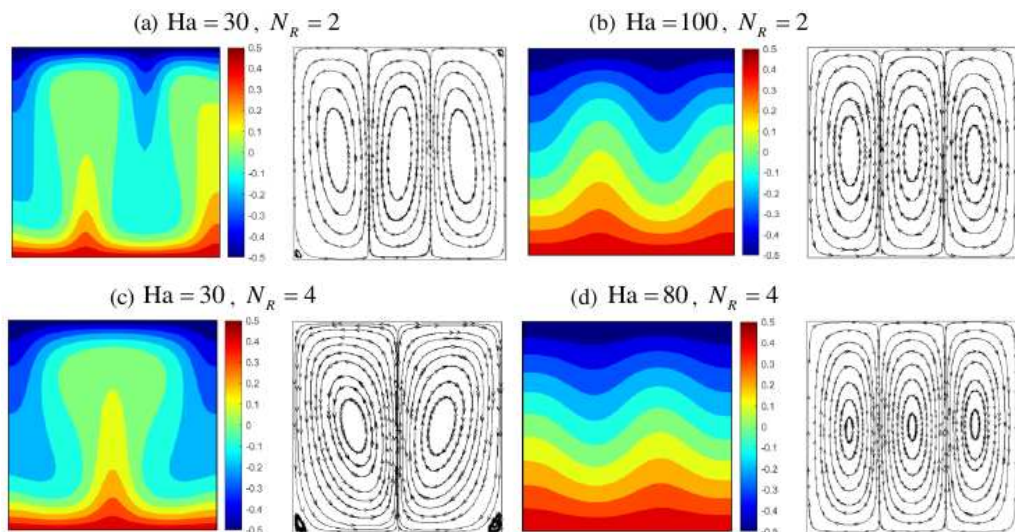


Fig. 5. Temperature distribution and streamlines at $Ra = 5 \times 10^5$.

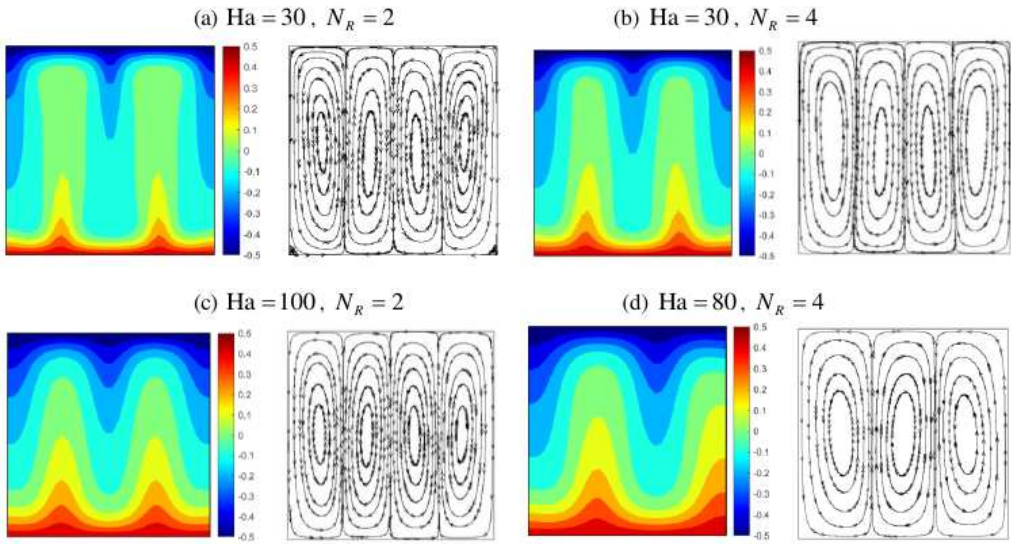


Fig. 6. Temperature distribution and streamlines for $Ra = 10^6$.

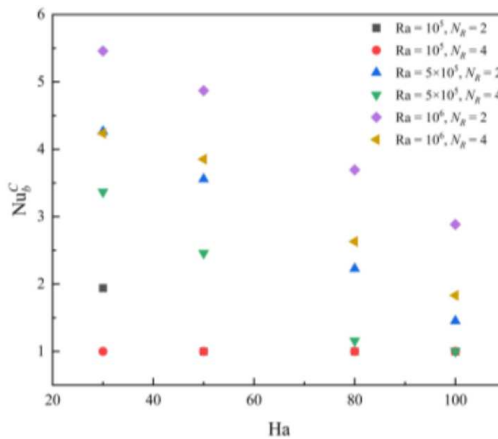


Fig. 7. Variations of Nu_b^C and Ha at different Ra .

increasing Ha , three long rolls are formed. From Fig. 6, we notice that four rolls exist in the bulk cavity at $Ha = 30$, $N_R = 2$ and three ones again appear at $Ha = 80$, $N_R = 4$. Fig. 7 shows the dependence of Nu_b^C on Ha at different values of Ra and N_R . At the same Ra and Ha , there is an obvious decreasing of Nu_b^C with increasing N_R . This can be explained by the fact that the radiative heat transfer near the hot wall becomes more significant when N_R increases, and, therefore, the convective heat transfer decreases. The temperature gradient of the fluid close to the bottom wall drops when more radiation participates. Fig. 8 show the dependence of Nu^C and Re on Ha at different values of Ra and N_R . We noticed that Nu^C and Re decreased to 1 and 0 at $Ra = 10^5$, $Ha = 30$ when N_R varied from 2 to 4, respectively. However, with $Ra = 5 \times 10^5$ and $Ra = 10^6$, Nu^C and Re increased with N_R when Ha was not so large. This can be explained as the fact that the driving effect of thermal radiation is sufficient to offset the dampening effect of the magnetic field resulting in stronger convective heat transfer over the whole system. Upon an increase of Ha , Nu^C and Re decreased.

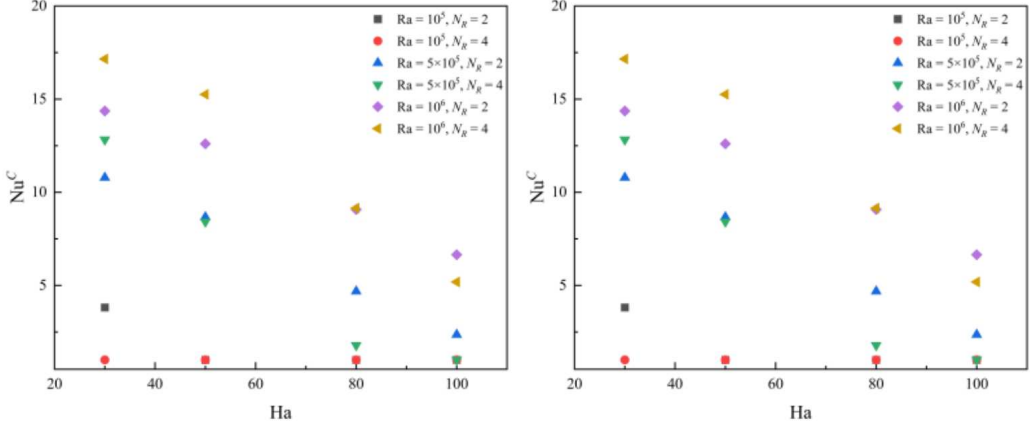


Fig. 8. Variations of Nu^C and Re along with Ha at different Ra .

3. Conclusions.

In the present work, we numerically studied the combined effects of the magnetic field and radiation on the heat transfer and fluid flow of molten salt using the collocation spectral method. The linear Rosseland approximation was adopted to simplify the computation of thermal radiation. We found that the convective heat transfer and fluid flow in the whole cavity were significantly influenced (enhanced or weakened) by the effects of radiation and magnetic field. Besides, it is worth mentioning that a corresponding experimental study is also in progress. The preliminary numerical results provide fundamental needs for the experiments set-up.

4. Acknowledgments.

This work was supported by the Natural Science Foundation of China (grant No. 51976021), Deutsche Forschungsgemeinschaft (grant No. 467227170) and China Scholarship Council (grant No. 202206060015).

References

- [1] S. ROSSELAND. *Theoretical Astrophysics: Atomic Theory and the Analysis of Stellar Atmospheres and Envelopes*. (Clarendon Press, Oxford, U.K., 1936).
- [2] R. ROPER, M. HARKEMA, P. SABHARWALL, C. RIDDLE, B. CHISHOLM, B. DAY, P. MAROTTA. Molten salt for advanced energy applications: A review. *Annals of Nuclear Energy*, vol. 169 (2022), p. 108924.
- [3] L. WANG, Q. YAN. Research progress of the application and properties of molten salt to solar thermal power. *Material Science*, vol. 5 (2015), pp. 72–78.
- [4] I. BELYAEV, E. BELAVINA, A. KOTLYAR, Y. LISTRATOV, V. SVIRIDOV. Heat transfer in mixed convection of molten salt in the presence of magnetic fields. *Technical Physics Letters*, vol. 45 (2018), pp. 499–502.
- [5] S. SMOLENSTEV, R. MIRAGHAIE, M. ABDOU. MHD effects on heat transfer in a molten salt blanket. *Fusion Science and Technology*, vol. 47 (2005), pp. 559–563.
- [6] J. GUO, Y. CHEN, J. HU, Z. XU, C. MA. Numerical study on the flow and heat transfer of molten salt in a horizontal pipe applied transverse magnetic field. *International Journal of Thermal Science*, vol. 192 (2023), p. 108416.

- [7] F. WANG, H. JIN, H. WANG, Z. CHENG, J. TAN, Y. YUAN, Y. SHANG, W. ZHANG. Radiative, conductive and laminar convective coupled heat transfer analysis of molten salts based on finite element method. *Applied Thermal Engineering*, vol. 131 (2018), pp. 19–29.
- [8] P. LI, X. LUO, L. CHEN, J. SONG, B. LI, C. KARCHER. Numerical research for the effect of magnetic field on convective transport process of molten salt in Rayleigh–Bénard system. *International Journal of Thermal Science*, vol. 195 (2024), p. 108605.
- [9] P. LI, J. CALMBACH, C. NAUMANN, C. RESAGK, C. CIERPKA, C. KARCHER. Experimental investigation and numerical analysis of convective heat and mass transport processes in salt melts affected by magnetic fields and thermal radiation. *tm-Technisches Messen*, vol. 18 (2024), pp. 1–20.
- [10] X. C HEN, Y. WU, C. WANG, X. WANG, C. MA. Flow and mixed convection heat transfer of Hitec salt in multi-sided heating pipes. *Sustainable Energy Technologies and Assessments*, vol. 47 (2021): 101375.
- [11] H. SHATNAWI, C. LIM, F. ISMAIL. Solar thermal power: appraisal of solar power towers. *MATEC Web of Conferences*, vol. 225 (2018): 04003.
- [12] M. XIE, Y. ZHU, Y. LIU, Y. YUAN, H. TAN. Measurement of spectral radiative characteristics of molten salt at high temperature using emission method. *Applied Thermal Engineering*, vol. 149 (2019): 1451–164.

Received 24.11.2024